Journal of The Electrochemical Society, **161** (4) E53-E60 (2014)
0013-4651/2014/161(4)/E53/8/$31.00 © The Electrochemical Society

Electrosynthesis and In Situ Spectroelectrochemistry of Conducting *o*-aminophenol-*p*-aminophenol Copolymers in Aqueous Solution

Jalal Arjomandi[z] **and Zahra Kakaei**

Department of Physical Chemistry, Faculty of Chemistry, Bu Ali Sina University, 65178 Hamedan, Iran

Copolymerization of *o*-aminophenol (*o*-AP) and *p*-aminophenol (*p*-AP) in aqueous sulfuric acid solution was electrochemically performed using cyclic voltammetry on gold electrode. Copolymerization was carried out at different feed concentrations of homo monomers. The obtained films were characterized with cyclic voltammetry, in situ resistivity measurements, in situ UV-Vis-spectroscopy, FT-IR spectroscopy, and scanning electron microscopy (SEM). Cyclic voltammetry study shows that the onset potentials for *o*-AP, *p*-AP and *o*-AP + *p*-AP are located at the different values. The results from the electrochemical copolymerization of *o*-AP with *p*-AP demonstrate that the CVs of copolymers films growth are different from those of homopolymers, and are strongly affected by the amount of monomers. The in situ resistivity of copolymers measured from −0.20 V to 0.95 V vs. SCE decreased with increasing the [*o*-AP]/[*p*-AP] concentration ratio. In situ UV-visible and ex situ FT-IR spectra of homopolymers and copolymers results show intermediate spectroscopic behavior between homopolymers and copolymers. SEM micrographs of the samples show fundamental differences between the morphology of the homo- and copolymers.

Manuscript submitted October 28, 2013; revised manuscript received December 30, 2013. Published February 3, 2014.

Aminophenols are interesting members of the class of substituted aniline. The hydroxyl group in the phenyl ring can be oxidized to quinine and quinine can be reduced again. Thus, unlike aniline and other substituted aniline, they have two groups (NH_2 and OH), which could be oxidized. Therefore, they could show electrochemical behavior resembling anilines[1–3] and/or phenols.[4,5] An important factor would be the relative position of the amino and hydroxyl group in the aromatic ring. The reported electrochemical properties of the three positional isomers (*ortho*, *meta* and *para*) are strongly different.[6] Several researchers have studied the electropolymerization of *ortho*, *meta* and *para* aminophenol on different electrode materials (platinum, gold, carbon, etc.) and solvents.[7–18] Poly (*o*-aminophenol) (P(*o*-AP)) has attracted most attention due to the formation of electro active polymer during its chemical and electrochemical oxidation. P(*o*-AP) has been investigated with electrochemical, spectroelectrochemical, and impedance measurements[19–23] and applied in sensors, biosensors and corrosion protection.[24–27] Many literatures are also available on electrochemical polymerization of poly(*p*-aminophenol) (P(*p*-AP)) and poly(*m*-aminophenol) (P(*m*-AP)).[11,13,18,28–30] Electro copolymerization offers the advantages of preparing a wide array of materials with redox activity, varying conductivity and stability. Electrochemical copolymerization of *ortho*, *meta* and *para* aminophenol with aniline have already been discussed and reported.[31–45] From those works, some approaches to improving the poly aniline properties were reported. The first approach was to synthesize polymers and copolymers from aniline and aniline derivatives with *ortho*, *meta* and *para* aminophenol monomers. The second was changing polymerization conditions of aniline or its derivatives. However, it is generally difficult to find polymerization or copolymerization conditions which are used to synthesize polymers having electrochemical and electric properties and stability better than polyaniline (PAn) itself. The third approach was to measured resistivity and optical properties. The resistivity of poly (aniline -co -*o*-aminophenol) and poly (aniline -co- *p*-aminophenol) are higher than that of polyaniline. The optical properties of different copolymers have been compared with homopolymers and correlated with the electrochemical and in situ conductivities. Finely, in order to obtain a desirable copolymer whose property is given better than that of parent PAn, electrochemical or chemical copolymerization of aniline and *o*-AP or aniline and *p*-AP were carried out and reported by researchers. This is because the copolymerization of aniline with *o*-AP or *p*-AP creates a possible way for preparing a new type copolymer with retains the good properties of PAn itself and also possesses new properties. The pH dependence of the electrochemical activity and effect of ratio concentration of aniline and *o*-AP or *p*-AP monomers in the feed on the rate of copolymerization and the electrochemical properties of the deposited polymers have been investigated and compared with those of homopolymers. PAn has little electro activity at pH ≥ 4, whereas copolymers of aniline with *o*-AP show electrochemical activity even at pH = 10.0. So, copolymerization has improved the pH dependence of the electrochemical activity.[46] In present paper, conducting P(*o*-AP), P(*p*-AP) and their copolymers (P(*o*-AP-co-*p*-AP)) were prepared by electrochemical method on gold electrode in sulfuric acid. According to our best knowledge, no reports are currently available for electro copolymerization of two aminophenol isomers together. The homopolymers and copolymers obtained were characterized with cyclic voltammetry (CV), in situ UV-Visible, ex situ FT-IR spectroscopy, in situ resistivity measurements and SEM analysis. As we know very well, the copolymerization of monomers like the preparation of a metallic alloy is able to change the properties of the homopolymers. So, it is very interesting to preparing a new aminophenol type copolymer and it's applies as a starting material to be coupled with polyaniline.

Experimental

Reagents and solvents.— The chemical used were of reagent grade. *o*-AP and *p*-AP (99%) were obtained from Merck and used without further purification. Sulfuric acid (Merck) was used as received. Doubly distilled water was used to prepare solutions.

Electrochemistry, UV–visible, and FTIR spectroscopy.— Cyclic voltammetry (CV) was performed using a Behpajoh model BHP/2062 and an Atolab model PGSTAT 20 potentiostat/galvanostat. A three-compartment electrochemical H cell with glass frit separators between the cell compartments was used for voltammetry studies. Working and auxiliary electrodes were gold sheets of ∼0.4 and 1.0 cm^2 surface area (from AZAR electrode), respectively. For UV– vis spectroscopy optically transparent ITO-coated glass sheets (surface area is 0.7 × 4.5 cm^2, Praezisions Glas & Optik, Germany, R = 20 ± 5 Ω cm^{-2}) were used as working electrodes in a standard 10-mm cuvette. A gold wire served as counter electrode, the reference electrode was connected via a plastic tube. The saturated calomel electrode (SCE) was used as reference electrode in all experiments. UV–vis spectra were recorded with the polymer and copolymer films deposited from the electrolyte solutions. A UV–vis spectrophotometer Perkin Elmer 55 OSD with a cuvette with the same solution and an uncoated ITO glass in the reference beam was used. Spectra were recorded at increasingly positive electrode potentials; in a few cases, spectra were recorded in the negative-going potential direction also in order to test reversibility. The stability of the optical response was checked frequently in the

[z]E-mail: jalal.arjomandi@s2004.tu-chemnitz.de

selected potential ranges. For in situ resistance measurements a band-gap gold electrode setup (from AZAR electrode) was used as working electrodes.[47–51] The two strips of the band-gap electrode are spaced apart only around 0.08–0.10 mm; this gap can easily be bridged by deposition of conducting polymers. The length of the gap is around 3–4 mm. The polymer films are deposited electrochemically on the electrode strips as desired, even very thin films usually form good bridges over the gap between the electrodes. Before each polymer deposition, the electrode was polished with fine emery paper (1,000 grit) and alumina (1 μm) to remove the previously deposited material, washed with water, and cleaned ultrasonically. The instrument for resistance measurement was made by Sama Research Center. Infrared spectra of dedoped samples were recorded on a Perkin Elmer FT-IRGX spectrometer using the KBr pellet technique. Films were scraped of the electrode, milled with KBr, and pressed into pellets.

P(o-AP), P(p-AP) and P(o-AP-co-p-AP) films electrosynthesis.— Monomers and electrolyte concentrations were, [*o*-AP] = 0.1 M, [*p*-AP] = 0.1 M, (P(*o*-AP-co-*p*-AP) (Cop. A) (1:1, 0.05 M-0.05 M), Cop. B (3:1, 0.075 M-0.025 M), Cop. C (1:3, 0.025 M-0.075 M) ratios of *o*-AP and *p*-AP solutions prepared in sulfuric acid ([H_2SO_4] = 0.5 M) separately. After vigorous mixing and nitrogen purging (10 min) electropolymerization was effected by scanning the electrode potential initially between $-0.20 < E_{SCE} < 0.95$ V at a scan rate 50 mV · s^{-1}. All the polymer films were transferred into a 0.50 M solution of H_2SO_4 to remove unreacted *orto* or *p*are-aminophenol, and then rinsed with doubly distilled water before use in the following characterization experiments.

Morphology.— The morphological study was carried out with a Hitachi S-4160 scanning electron microscope (SEM). For this purpose, films were peeled from the gold electrode and attached with graphite glue to a copper holder.

Results and Discussion

Electrochemical copolymerization of o-AP and p-AP.— The cyclic voltammograms for electrosynthesis of the P(*o*-AP), P(*p*-AP) and P(*o*-AP-co-p-AP) (Cop. A, B, C) films on gold electrode between $-0.20 < E_{SCE} < 0.95$ V at a scan rate 50 mV · s^{-1} are shown in Fig. 1.

The first CV of *o*-AP shows two anodic peaks and one cathodic peak (Fig. 1A). The peak observed at 0.61 V is due to the oxidation of hydroxyl group in phenyl ring,[36] and the other anodic weak peak at 0.81 V is caused by the oxidation of amino group in phenyl ring of *o*-AP, which could be ascribed to the formation of P(*o*-AP).[7,34,52] For the second cycle, two redox peaks appears at 0.17 V and 0.33 V, which is caused by the formation of a cyclic dimmer of *o*-AP (3-aminophenoxazone). This pair of redox peak is due to the oxidation

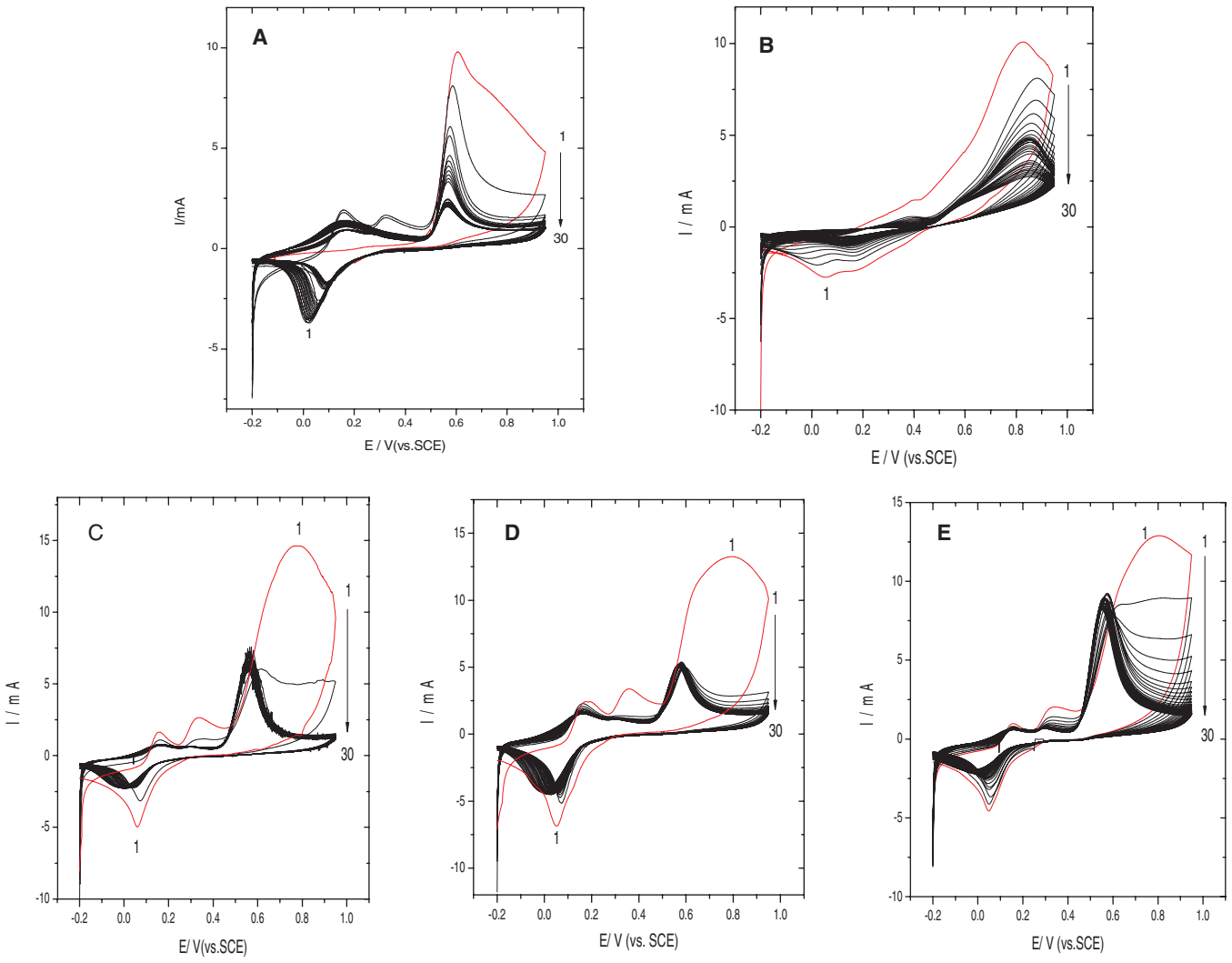

Figure 1. CVs during formation of (A) P(*o*-AP), (B) P(*p*-AP), (C) Cop. A, (D) Cop. B and (E) Cop. C in [H_2SO_4] = 0.5 M, [*o*-AP] = 0.1 M, [*p*-AP] = 0.1 M, (P(*o*-AP-co-*p*-AP) (Cop. A) (1:1), Cop. B (3:1) and Cop. C (1:3) ratios of *o*-AP and *p*-AP solutions between −0.20 and 0.95 V at a scan rate 50 mV · s^{-1}, respectively. Dash line is first cycle.

and reduction of P(*o*-AP), indicating the formation of polymer. After the continuous potential scanning, the oxidation current decreases quickly with increase the number of potential cycles and polymer film grows with time. Thus, monomer is firstly oxidized to form cycle dimmer and then, the dimmer plays a role of a monomer in the following polymerization.[16,34] After 30 potential cycles, a brownish thin film was found on the working electrode. However, at rather high anodic potential (i.e. 1.10 V) and on further potential cycling up to 100 cycles, no thick film growth was observed on the electrode surface except brownish soluble products in the electrolytic cell. This might be due to simultaneous degradation of the oligomeric or polymeric materials at rather high anodic potential.[34,54] The first CV of pure P(*p*-AP) (Fig. 1B) shows two anodic peaks at about 0.41 V and 0.81 V which could be ascribed to the formation of the monomer radicals. The shoulder peak could be due to that the radical undergoes an electron/proton reaction to *para*-quinonimine, which could diffuse toward the bulk solution and be subsequently hydrolyzed into *para*-benzoquinone.[44] Maia and Menezes[53] suggest that, the adsorption of P(*o*-AP) and the first one-electron transfer take place in the first oxidation peak potential region and its vicinity; after that, the adsorbed radical remains adsorbed on the electrode surface and undergoes a second one-electron transfer and loss of second proton to yield *para*-quinonimine. A 1, 4-addition of monomer to *para*-quinonimine or *para*-benzoquinone occurs rapidly to yield amine-substituted quinones or amine-substituted hydroquinones for the first cycle. After the continuous potential scanning, the products can be oxidized and react with monomer via 1, 4-addition and a single anodic peak appears at more than 0.85 V. The P(*p*-AP) film formed and grows with time and after 30 cycles, violet thin film was found on the working electrode. Like P(*o*-AP), no thick film growth was observed on the electrode surface. The violet soluble product in the electrolyte cell was observed at higher potential cycling. As it is well known polymeric materials are susceptible of degradation, especially after continuous cycling or after to be subjected to high positive potentials.[54] Fig. 1C shows CVs for electrolysis of an aqueous solution containing *o*-AP and *p*-AP (1:1) and 0.50 M H_2SO_4. It is clear that the CVs in Fig. 1C are different from those in Fig. 1A and 1B. For the first cycle in Fig. 1C, there are three anodic peaks, which began to form at about 0.16, 0.33 V and 0.77 V, respectively. The anodic broad peak potential between 0.70 to 0.84 V are shifts to 0.61 V for the second cycle, and then these anodic peak potential decrease markedly in the subsequent cycles until 0.55 V. A broad peak between 0.70–0.84 V may indicate the formation of copolymer. However, the shape of CVs may indicate that *p*-AP inhibits the copolymerization of *o*-AP with *p*-AP. The two redox couples at about 0.16 and 0.33 V could be caused by the redox of the copolymer. During the electrolysis, the redox couple at about 0.16 V may also be attributed to the reduction / re oxidation of quinonimine, which is the product of the imine hydrolysis reactions. After 30 potential cycles, a brownish violet thin film (Cop. A) was found on the working electrode. Fig. 1D shows CVs for electrolysis of an aqueous solution containing *o*-AP and *p*-AP (3:1) and 0.50 M H_2SO_4. It is clear that the CVs in Fig. 1D are much similar to P(*o*-AP) in Fig. 1A, since *o*-AP exhibited higher effect on the copolymerization in the former than the one in the latter. For the first cycle in Fig. 1D, there are two anodic peaks, which began to form at about 0.35 and 0.81 V, respectively. The anodic broad peak potential between 0.60 to 0.95 V are shifts to 0.62 V for the second cycle, and then these anodic peak potential decrease in the subsequent cycles until 0.57 V. After 30 potential cycles, a brownish thin film (Cop. B) was found on the working electrode. Fig. 1E shows CVs for electrolysis of an aqueous solution containing *o*-AP and *p*-AP (1:3) and 0.50 M H_2SO_4. For the first cycle in Fig. 1E, there are three anodic peaks, which began to form at about 0.15, 0.35 and 0.80 V, respectively. The anodic broad peak potential between 0.70 to 0.90 V are shifted to sharp peak at around 0.60 V for the third cycle, and then these anodic peak potential decrease in the subsequent cycles until 0.55 V. A peak at about 0.15 V may indicate that the formation of copolymer. After 30 potential cycles, a violet thin film (Cop. C) was found on the working electrode. The differences between second anodic and cathodic peak for the thirty cycles ($\Delta E_P = E_{Pa}\text{-}E_{Pc}$) of the P(*o*-AP), P(*p*-AP), Cop. A, Cop. B and Cop. C are 0.474, 0.695, 0.532, 0.578 and 0.601 V, respectively. The results from the electrochemical copolymerization of *o*-AP with *p*-AP demonstrate that the CVs of copolymers films growth are different from those of homopolymers, and are strongly affected by the amount of *o*-AP or *p*-AP. Thus, copolymerizations under the low concentrations of *p*-AP or *o*-AP are favorable to the formation of the Cop. B or Cop. C. The CVs of the resulting polymer and copolymer films were measured in 0.5 M sulfuric acid solution on gold electrode between $-0.20 < E_{SCE} < 0.95$ V at a scan rate of 50 $mV \cdot s^{-1}$ (Fig. 2).

As seen in Fig. 2A and 2B, there are two anodic peaks and two corresponding cathodic peaks at different potential positions. In the case of Fig. 2C, 2D and 2E, two separate redox couple on curves, which are very similar in shapes. However, the first cathodic peak potentials and currents for copolymers are located at different values. The differences between second anodic and cathodic peak ($\Delta E_P = E_{Pa}\text{-}E_{Pc}$) of the Cop. A, Cop. B and Cop. C are 0.666, 0.720 and 0.764 V, respectively. The differences between the anodic and cathodic peaks in copolymers are depending on different experimental conditions i.e. different monomer concentration, employed during electropolymerization process.

In situ resistivity of homo polymer and copolymer films.— The resistivity versus the applied electrode potential plot of P(*o*-AP) and P(*p*-AP) films in 0.5 M H2SO4 is displayed in Fig. 3A–3B. P(*o*-AP) shows two changes in resistivity (Fig. 3A).

When the applied potential is increased, the resistivity of the polymer decreases sharply by 0.15 orders of magnitude at 0.10 V and then increases again at 0.60 V. When the potential shift direction is reversed from 0.90 to −0.20 V, the resistivity of polymer is nearly constant up to 0.60 V and increases up to 0.30 V and than decreased by 0.6 orders of magnitude. Minimum resistivity was observed in the potential region between −0.10 and 0.10 V. The lower in situ conductivity of P(*o*-AP) has been reported[55,56] and the mechanisms of conductance discussed by Goyette and Leclerc previously.[57] According with these authors, in the partially oxidized polymer some protonated imines may exist and act as charge carriers for a structurally related poly(2,3-diaminotoluine) with one broad redox process. In our case too, only one redox pair in aqueous acidic solution was observed during cycle by cycle electro synthesized (see Fig. 2A). Thus, lower in situ conductivity is predictable for polymer samples. For P(*p*-AP) film, minimum resistivity was observed in the potential region between 0.05 and 0.35 V, but is lower roughly by 0.15 orders of magnitude as compared to P(*o*-AP) (Fig. 3B). Here also, two changes in resistivity are observed. At a more positive electrode potential, the resistivity decreased from 0.00 to 0.40 V and than increased up to 0.80 V. During the negative going potential scan, the resistivity it returned to the initial value from 0.40 V by decreasing about 0.35 orders of magnitude. Results obtained with copolymers (Cop. A, B, and C) are shown in Fig. 3C–3E. With increases the applied potential from −0.20 to 0.35 V, the resistivity of Cop. A is decreases in −0.15 V and then increases at 0.35 V. Its resistivity is higher than that of P(*p*-AP) by 0.2 orders of magnitude. Minimum resistivity can be observed in the range between 0.20 V and 0.40 V. Like Cop. A, two changes can be observed with Cop. B and C. The higher resistivity of Cop. C is due to increase of the concentration of *p*-AP in the co monomer feed and may suggest the incorporation of more *p*-AP monomer units in the resulting copolymer film. All copolymers have similar (Cop. B) or higher (Cop. A and C) resistivity than P(*o*-AP) and P(*p*-AP) films. In addition, the resistivity of copolymers here, are higher than that of poly (aniline-co-*o*-aminophenol), poly (aniline-co- *p*-aminophenol) and polyaniline itself.[55,56]

In situ UV-visible and ex situ FT-IR spectroelectrochemistry.— The in situ UV-visible spectra of all films in a solution of sulfuric acid at different applied electrode potentials are shown in Fig. 4. Films were prepared potentiodynamically by cycling the electrode potential in the range of $-0.20 < E_{SCE} < 0.95$ V on ITO coated glass electrode from a solution containing 0.05 M *o*-AP in 0.5 M sulfuric acid solution.

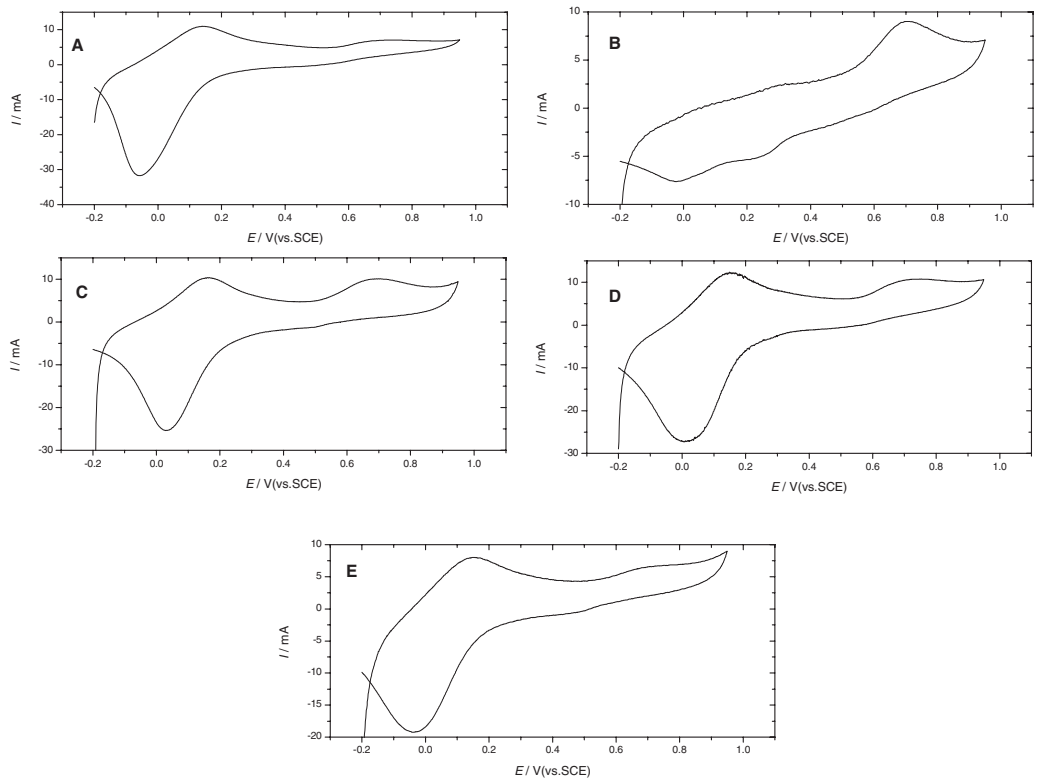

Figure 2. CVs of (A) P(*o*-AP), (B) P(*p*-AP), (C) Cop. A, (D) Cop. B and (E) Cop. C in $[H_2SO_4] = 0.5$ M, $-0.20 < E_{SCE} < 0.95$ V, gold electrode, scan rate was 50 mV · s^{-1}, respectively.

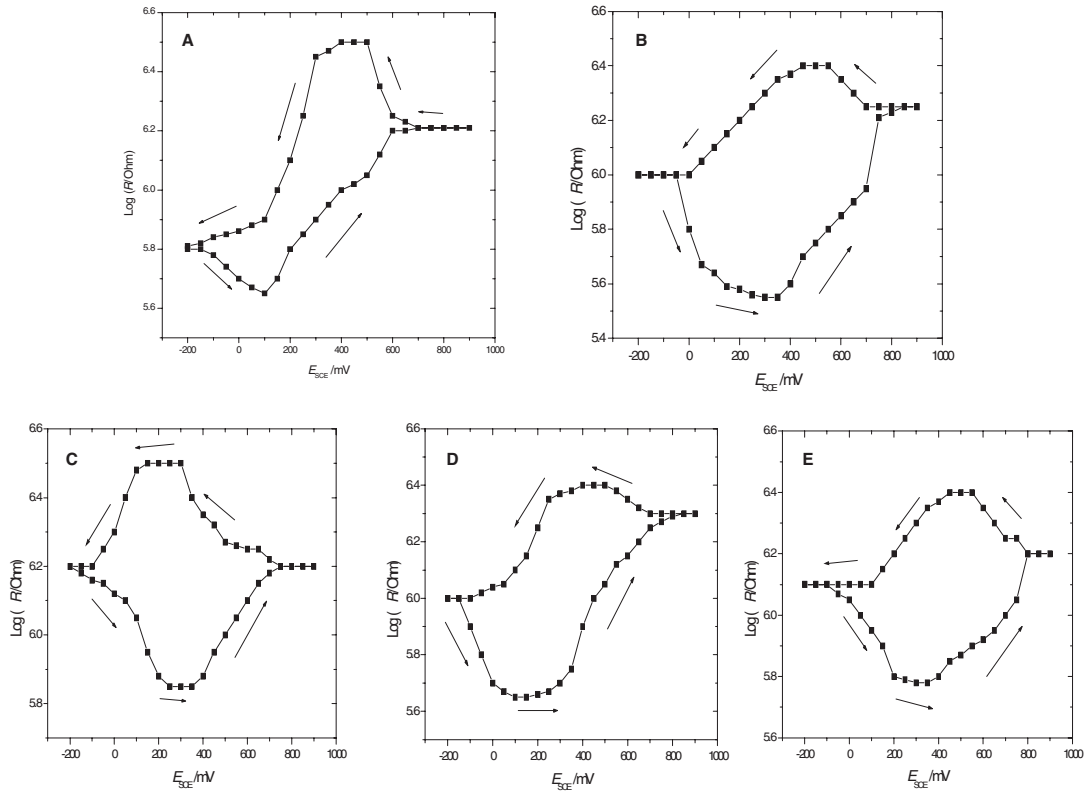

Figure 3. Resistivity vs. electrode potential data for (A) P(*o*-AP), (B) P(*p*-AP), (C) Cop. A, (D) Cop. B and (E) Cop. C in $[H_2SO_4] = 0.5$ M. Films prepared potentiodynamically by cycling the potential between −0.20 V and 0.95 V from different monomer and co monomer concentrations in $[H_2SO_4] = 0.5$ M, gold electrode, scan rate was 50 mV · s^{-1}, respectively.

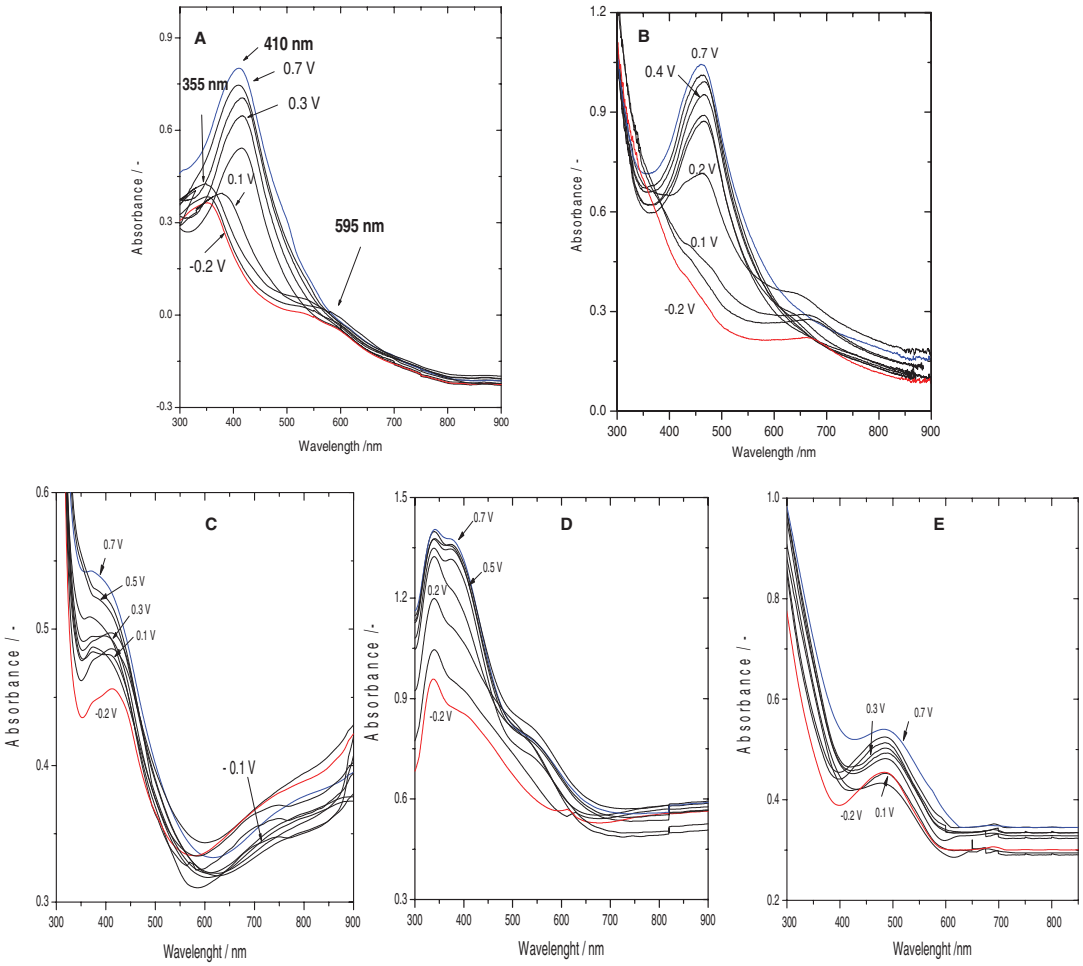

Figure 4. In situ UV-Vis-spectra for (A) P(*o*-AP), (B) P(*p*-AP), (C) Cop. A, (D) Cop. B and (E) Cop. C in $[H_2SO_4] = 0.5$ M. Films in a solution of $[H_2SO_4] = 0.5$ M deposited potentiodynamically between −0.20 V and 0.95 V on ITO.

The in situ UV-visible spectra of P(*o*-AP) (Fig. 4A) presents three absorption bands at about 355, 410 and 595 nm. These bands have been reported and discussed at about 350, 410 and 610 nm in the potentiodynamically prepared P(*o*-AP) by Shah and Holze.[31] The absorption band at 350 nm corresponds to the totally reduced state of the polymer. With increasing the applied potential up to 0.70 V, the absorption band at 350 nm shifts to broad band at about 410 nm, which correspond to the phenoxazine of the polymer. The absorption band at about 595 nm was observed only in the reduced state of the polymer between −0.20 to 0.10 V and disappears with an increase of the applied potential up to 0.7 V.[58] Fig. 4B shows in situ UV-visible spectra of P(*p*-AP). Two absorptions bands located at 455 and 650 nm are observed in the spectra. The absorption band at about 650 nm was observed only in the reduced state of the polymer between −0.20 to 0.20 V and disappears with an increase of the applied potential up to 0.70 V. Hassan et al.[59] report that *para*-benzoquinone has a maximum absorption at 430 nm and readily reacts with aliphatic primary and secondary amines in organic solvents to give an intense color with a large absorption band at 510 nm. After the electro oxidation of P(*p*-AP), a 1, 4-addition reaction of monomer to *para*-benzoquinone may occurs.[53] The maximum absorption at 465 nm observed at 0.70 V for P(*p*-AP) in the present work. These maximums absorption can be related to the formation of localized polarons in the film chain, due to the oxidation process. The in situ UV-visible spectra of copolymers (Cop. A, Cop. B and Cop. C) are shown in Fig. 4C–4E. The obvious spectral differences between homo- and copolymers as well as between the different copolymers indicate the effect of concentration of co monomers in the polymer backbone. For Cop. B (Fig. 4D), three absorptions bands at 340, 410 and 560–630 nm are observed in the spectra. During oxidation of the copolymer film, an increases of absorbance can be observed like with P(*o*-AP). The absorption band at about 630 nm was observed only in the reduced state of the polymer between −0.20 to 0.00 V and shifted negatively with an increase of the applied potential up to 0.70 V to 560 nm. In the case of Cop. C (Fig. 4E), when the concentration of *p*-AP units is increased, an increase in the absorbance between 480–520 nm oxidation can be observed. The absorption band at about 650 nm for P(*p*AP) was observed here in the reduced state of the copolymer at about 620 nm (between −0.20 to 0.00 V) and disappears with an increase of the applied potential up to 0.70 V. At intermediate concentrations of the monomers (1:1, Cop. A), the behavior of the film is similar to both P(*o*-AP) and P(*p*-AP) (Fig. 4C). The absorption band at about 420 nm was observed in the reduced state of the copolymer between −0.20 to 0.30 V and shifted negatively with an increase of the applied potential to 370 nm. Like other copolymers, the absorption band at about 720 nm was observed in the reduced state of the Cop. A at about 720 nm (between −0.20 to 0.20 V) and disappears with an increase of the applied potential. In comparison with homo polymer films upon oxidation, the nearly sharp bands at about 410 nm (P(*o*-AP)) and 455 nm (P(*p*-AP)) are shifted to a broad band between 370–420 nm in Cop. A. The apparent differences in band shapes and developments as a function of electrode potentials may suggest copolymer formation instead of formation of a mixture of homopolymers. Fig. 5 shows the FT-IR transmission spectra of homo polymer and copolymer films in the ranges of 400–2000 cm^{-1} (Fig. 5A–5E) and 1000–1650 cm^{-1} (Fig. 5F).

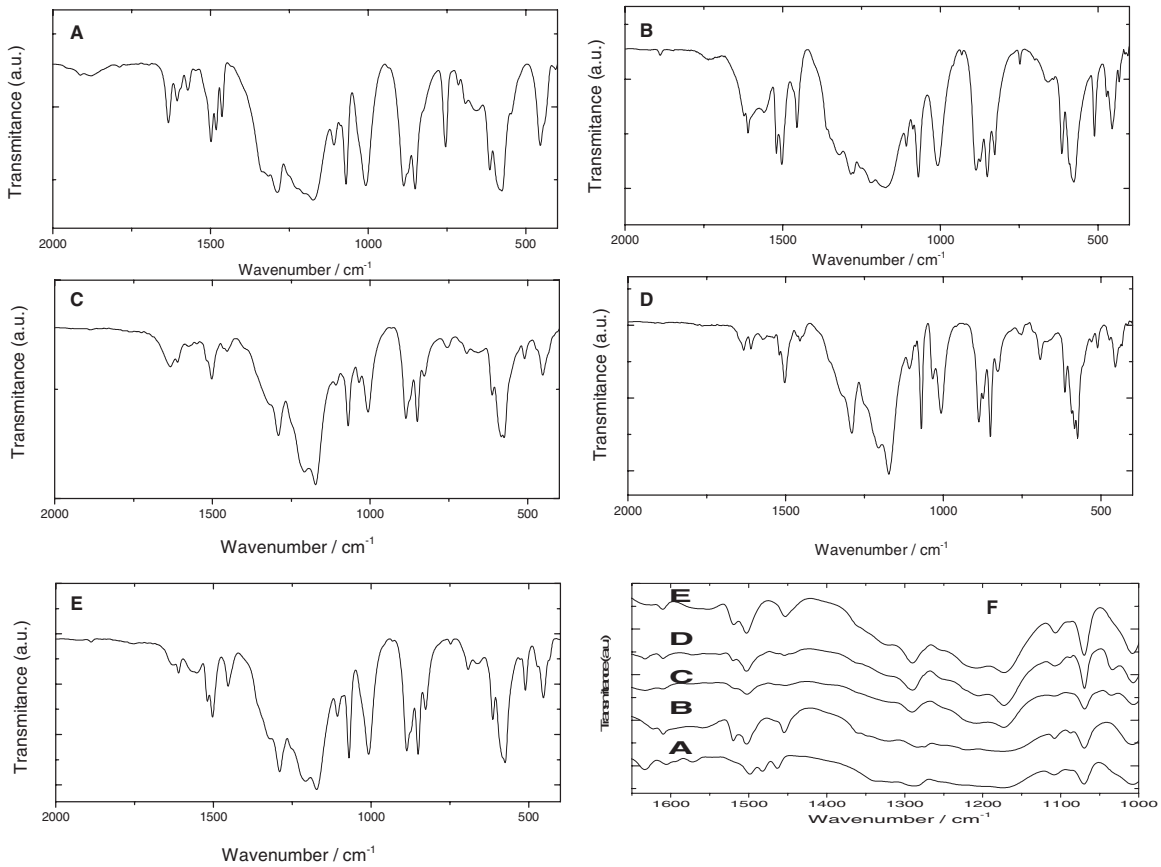

Figure 5. FTIR spectra of (A) P(*o*-AP), (B) P(*p*-AP), (C) Cop. A, (D) Cop. B, (E) Cop. C and (F) all sample films.

The characteristic vibrational bands associated with P(*o*-AP) and P(*p*-AP) present in P(*o*-AP-co-*p*-AP) copolymer films with a considerable shift and different intensities, which are indicates the synthesis of copolymers from two monomers. As shown in Fig. 5A for P(*o*-AP), the sharp bands at about 1502, 1481 and 1462 cm^{-1}, which can be ascribed to the aromatic C=C stretching vibration or ring C=C vibration of meta-disubstituted benzenes,[60] indicates that the oxidation of P(*o*-AP). The peak at 1292 is ascribed to O–H deformation vibration of phenols.[61,62] The bands at 1340 cm^{-1} (accompanying with 1296 cm^{-1}) is assigned to C=N or C–N stretching of quinoid rings. The band at 1605 cm^{-1} has contributions from two bands at 1574 and 1633 cm^{-1} and could be assigned to a quinoid ring or C=N stretching vibration in the phenoxazine units produced upon complete polymer oxidation. In FT-IR spectra of P(*o*-AP), no characteristic band at about 1680 cm^{-1} (C=O stretching vibration)[61,62] was observed, which suggesting that P(*o*-AP) may be formed through the $–NH_2$ groups rather than the –OH groups.[63] Three peaks of P(*o*-AP) at about 1174, 1109 and 1066 cm^{-1} are assigned to HSO_4^- and SO_4^{2-} ions.[64] This means that the ions have been doped into the polymer film during the electro polymerization process. Fig. 5B shows FT-IR spectra of P(*p*-AP). The C=O stretching vibration peak appears at 1610 cm^{-1} revealing that some of –OH side groups in the polymer have been oxidized. The band appears at 1555 cm^{-1} is assigned to the C=N formation. A sharp band at 1505 cm^{-1} due to stretching vibrations of N–H in second amine –NH– groups, indicates that the polymerizing chains grow through the amino groups.[44] Three peaks at 1503, 1450 and 1397 cm^{-1} are assigned to phenyl ring stretching vibrations. The broad peaks at about 1282 and 1218 cm^{-1} are due to a mixture of phenyl-O stretching vibration and O-H vibrations. Like P(*o*-AP), three peaks at about 1174, 1106 and 1072 cm^{-1} are assigned to HSO_4^- and SO_4^{2-} ions.[61] However, the peaks at 1174 and 1106 cm^{-1} may are assigned to C-H in plane deformation and C-N stretching vibration.[53] Furthermore, the peaks at about 886, 849 and 827 cm^{-1} suggest a 1, 2, 4 substitution pattern in polymer. The IR spectrum of copolymers shows in Fig. 4C–4E. The spectroscopic behavior of Cop. B and Cop. C (Fig. 5D and 5E) are similar to the P(*o*-AP) and P(*p*-AP) films. However, slightly shift in the bands were observed for copolymers at the comparing with homopolymers (see Fig. 5F). The band at 1605 cm^{-1} and 1633 cm^{-1} in P(*o*-AP), which are assigned to a quinoid ring or C=N stretching vibration in the phenoxazine units observed at 1610 and 1632 cm^{-1} in Cop. B. Furthermore, the increase in its intensity with an increase of the concentration of *o*-AP in the co monomer feed suggests the incorporation of more *o*-AP units in the resulting copolymer. In the case of Cop. C (with high amount of *p*-AP in the co monomer feed), the peak at 1450 cm^{-1} due to phenyl ring stretching vibrations for P(*p*-AP) are take place at 1455 cm^{-1} in copolymer. The FT-IR spectrum of Cop. A (Fig. 5C) (an equimolar concentration of monomers) shows the intermediate spectroscopic behavior between homopolymers and copolymers. The above results demonstrate that the IR spectrum of copolymers are different from those of P(*o*-AP) and P(*p*-AP) films. This means that an electrochemical copolymerization of monomer films took place in this work. The major infrared bands and their assignments for P(*o*-AP), P(*p*-AP), Cop. A, Cop. B and Cop. C are shown in Table I.

Morphology of homo polymer and copolymer films.— The morphology of polymer and copolymer films was measured using SEM and displayed in Fig. 6.

Fig. 6A and 6B are the morphology of the homopolymers films, which are constructed of the interwoven fibers with different diameters and lengths. The space between long fibers is very large compared to size or radii of anions (SO_4^{-2}) and thus the ions can be permitted into the inner polymer film during the doping process. The morphology of Cop. A (Fig. 6C) is different from homopolymers and shows

Table I. Major infrared bands and their assignments for P(*o*-AP), P(*p*-AP), Cop. A, Cop. B and Cop. C.

			Wavenumbers/cm^{-1}		
Description	P(o-AP)	P(p-AP)	Cop. A	Cop. B	Cop. C
C=O O-H stretching (oxidized)	1605	1610	1605	1609	1608
Quinoid ring C=N stretching C–N or C=N stretching	1633 1605 1555 1340	1627 1608 1557 1317	1631 1603 1561 1327	1629 1607 1570 1323	1627 1610 1562 1326
Aromatic C=C stretching ring C=C stretching vibration of meta-disubstituted benzens N-H stretch of second amino group	1502 1481 1462	1505 1450 1397	1501 1454	1501 1455	1500 1453
O-H deformation vibration of phenols	1292	1282 1218	1292 1211	1292 1203	1291 1206
HSO4-, SO4- C-H in plan deformation C-N stretching	1174 1109 1066	1174 1106 1072	1170 1102 1068	1172 1105 1072	1171 1109 1070

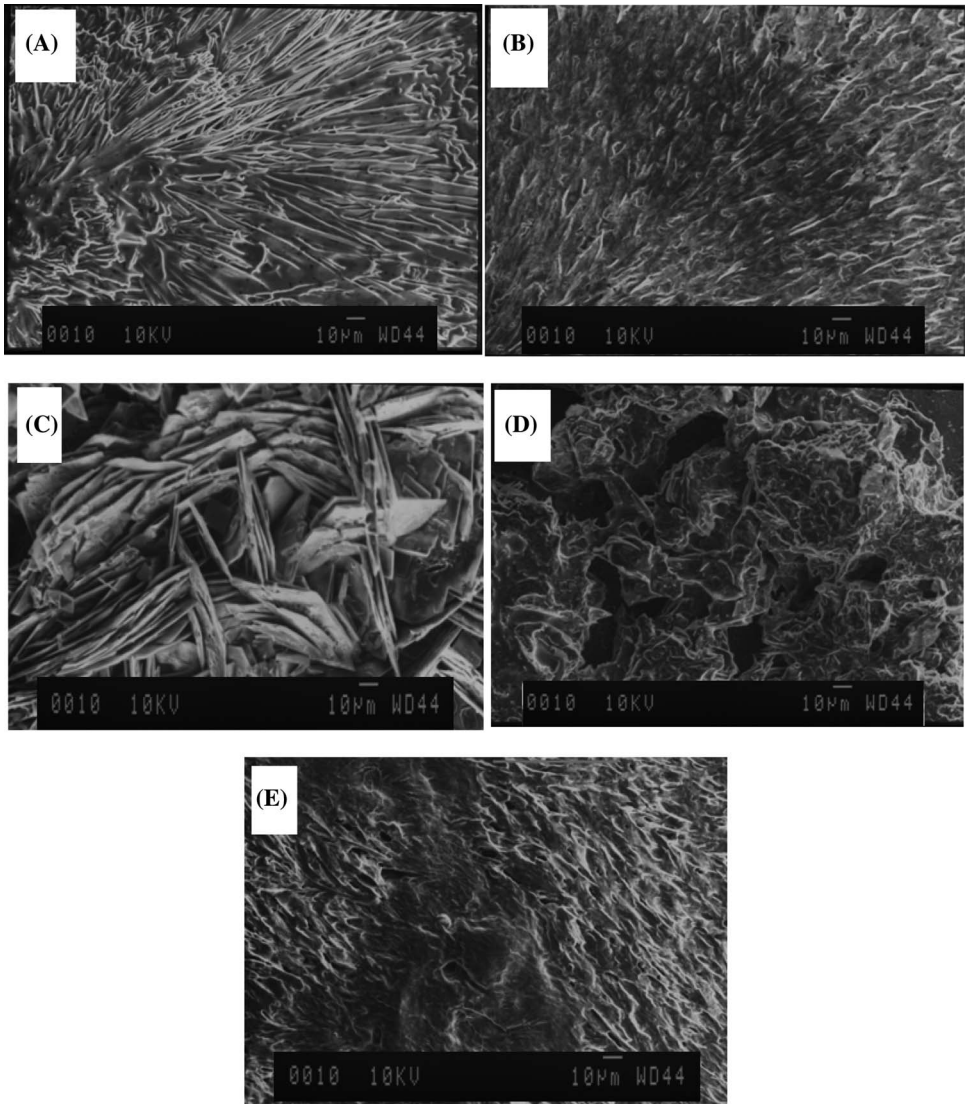

Figure 6. SEM micrographs of (A) P(*o*-AP), (B) P(*p*-AP), (C) Cop. A, (D) Cop. B and (E) Cop. C films.

the unique broad plate fibers with a good free space between them. As the concentration ratio of *o*-AP to *p*-AP in a mixture increased, the morphology of the copolymer (Fig. 6D) change to morphology of P(*o*-AP) and vice versa (Fig. 6E). Different morphology is caused by the polymerization or copolymerization rates and nature of the polymer films. When the polymerization rate is fast, high amounts of the polymer nuclei formed, followed by the copolymerization on the copolymer nuclei, which results in the continuous growth of the copolymer particles and thus, the changes of the morphology may occurs. Moreover, the lower resistivity of copolymers than that of homopolymers indicates that homopolymers have lower resistivity than corresponding copolymers. The changes in the resistivity and morphology of the copolymers with the composition of the mixture may shows that the composition of the Cop. B and Cop. C are dependent on the concentration ratio of the monomers.[65] In addition, the change in the concentration of monomers in the feed before electropolymerization is related to the change in the morphology and properties of the resulting copolymers.

Conclusions

Poly(o-aminophenol), poly(p-aminophenol) and poly(*o*-aminophenol-co-*p*-aminophenol) were electrochemically synthesized using potential cycling in sulfuric acid solution on gold electrode. The experimental results may demonstrate that the concentration ratio of each monomer to others in a mixture strongly influences on the electrochemical properties of the copolymer, in situ conductivity, in situ UV-visible and morphology.

Acknowledgments

This work was sponsored by Bu Ali Sina University; we thank F. Hosseini (Sama Research Center) for her help in making required instruments for measuring the in situ resistivity and also thank AZAR electrode for preparing all electrodes.

References

1. H. Yang and A. J. Bard, *J. Electroanal. Chem.*, **339**, 423 (1992).
2. N. Yamada, K. Teshima, N. Kobayashi, and R. Hirohashi, *J. Electroanal. Chem.*, **394**, 71 (1995).
3. J. Chiang and A. G. MacDiarmid, *Synth. Met.*, **13**, 193 (1986).
4. M. Gattrell and D. W. Kirk, *J. Electrochem. Soc.*, **139**, 2736 (1992).
5. R. Lapuente, F. Cases, P. Garces, E. Morallon, and J. L. Vazquez, *J. Electroanal. Chem.*, **451**, 163 (1998).
6.
7. H. J. Salavagione, J. Arias, P. Garcés, E. Morallón, C. Barbero, and J. L. Vázquez, *J. Electroanal. Chem.*, **565**, 375 (2004).
8. C. Barbero, J. Zerbino, L. Sereno, and D. Posadas, *Electrochim. Acta*, **32**, 341 (1987).
9. T. Ohsaka, S. Kunimura, and N. Oyama, *Electrochim. Acta*, **33**, 639 (1988).
10. A. Guenbour, A. Kacemi, A. Benbachir, and L. Aries, *Prog. Org. Coat.*, **38**, 121 (2000).
11. S. Taj, M. F. Ahmed, and S. Sankarapapavinasam, *J. Electroanal. Chem.*, **338**, 347 (1992).
12. O. I. Konopelnik, O. I. Aksimentyeva, and M. Y. Grytsiv, *Mater. Sci.*, **20**, 49 (2002).
13. J. Schwarz, W. Oelßner, H. Kaden, F. Schumer, and H. Hennig, *Electrochim. Acta.*, **48**, 2479 (2003).
14. F. Gobal, K. Malek, M. G. Mahjani, M. Jafarian, and V. Safarnavadeh, *Synth. Met.*, **108**, 15 (2000).
15. C. Barbero, J. J. Silber, and L. Sereno, *J. Electroanal. Chem.*, **263**, 333 (1989).
16. A. Q. Zhang, C. Q. Cui, Y. Z. Chen, and J. Y. Lee, *J. Electroanal. Chem.*, **373**, 115 (1994).
17. R. I. Tucceri, *J. Electroanal. Chem.*, **562**, 173 (2004).
18. S. Taj, M. F. Ahmed, and S. Sankarapapavinasam, *Synth. Met.*, **52**, 147 (1992).
19. J. M. Ortega, *Thin Solid Films*, **371**, 28 (2000).
20. A. Guenbour, A. Kacemi, A. Benbachir, and L. Aries, *Prog. Org. Coat.*, **38**, 121 (2000).
21. K. Jackowska, J. Bukowska, and A. Kudelski, *Pol. J. Chem.*, **30**, 825 (1994).
22. C. Barbero, J. Zerbino, L. Sereno, and D. Posadas, *Electrochim. Acta*, **32**, 693 (1987).
23. C. Barbero, R. I. Tucceri, D. Posadas, J. J. Silbero, and L. Sereno, *Electrochim. Acta*, **40**, 1037 (1995).
24. P. Dawei, C. Jinhua, Y. Shouzhuo, T. Wenyan, and N. Liha, *Anal. Sci.*, **21**, 367 (2005).
25. A. Guenbour, A. Kacemi, and A. Benbachir, *Prog. Org. Coat.*, **39**, 151 (2000).
26. A. E. Radi, J. M. Montornes, and C. K. Osullivan, *J. Electroanal. Chem.*, **587**, 140 (2006).
27. H. M. Nassef, A,-E. Radi, and C. K. Osullivan, *J. Electroanal. Chem.*, **592**, 139 (2006).
28. S. Eddy, K. Warriner, I. Christie, D. Ashworth, C. Purkiss, and P. Vadgama, *Biosensor Bioelectron.*, **10**, 831 (1995).
29. E. Ekinci, A. A. Karagozler, and A. E. Karagozler, *Electroanalysis*, **8**, 571 (1996).
30. L. I. Halaoui, H. Sharifian, and A. J. Bard, *J. Electrochem. Soc.*, **148**, E386 (2001).
31. A. A. Shah and R. Holze, *Synth. Met.*, **156**, 566 (2004).
32. A. A. Shah and R. Holze, *Electrochim. Acta*, **52**, 1374 (2006).
33. M. L. Liu, M. Ye, Q. Yang, Y. Y. Zhang, Q. J. Xie, and S. Z. Yao, *Electrochim. Acta*, **52**, 342 (2006).
34. L. Zhang and J. Lian, *J. Electroanal. Chem.*, **611**, 51 (2007).
35. A. A. Shah and R. Holze, *J. Solid State Electrochem.*, **11**, 38 (2006).
36. S. Mu, *Synth. Met.*, **143**, 259 (2004).
37. J. Zhang, D. Shan, and S. L. Mu, *Electrochim. Acta*, **51**, 4262 (2006).
38. J. Zhang, D. Shan, and S. L. Mu, *Polymer*, **48**, 1269 (2007).
39. J. Zhang, D. Shan, and S. L. Mu, *J. Power Sources*, **161**, 685 (2006).
40. S. L. Mu and C. Chen, *J. Phys. Chem. B*, **111**, 6998 (2007).
41. J. Zhang, D. Shan, and S. L. Mu, *Front. Biosci.*, **12**, 783 (2007).
42. K. D. Seo, K. P. Lee, A. I. Gopalan, S. J. Chung, Y. T. Lim, and S. H. Choi, *Sensors*, **7**, 719 (2007).
43. Y. Zhang, S. Mu, B. Deng, and J. Zheng, *J. Electroanal. Chem.*, **641**, 1 (2010).
44. C. Chen, C. Suna, and Y. Gao, *Electrochimica Acta*, **53**, 3021 (2008).
45. C. Chen, C. Sun, and Y. Gao, *Electrochemistry Communications*, **11**, 450 (2009).
46. C. Chen, C. Sun, and Y. Gao, *Electrochimica acta*, **54**, 2575 (2009).
47. R. Holze and J. Lippe, *Synth Met.*, **38**, 99 (1990).
48. S. Bilal and R. Holze, *J Electroanal Chem.*, **592**, 1 (2006).
49. J. Arjomandi and R. Holze, *J Solid State Electrochem.*, **11**, 1093 (2007).
50. J. Arjomandi and R. Holze, *Synth Met.*, **157**, 1021 (2007).
51. J. Arjomandi and R. Holze, *J. Solid State Electrochem.*, **17**, 1881 (2013).
52. C. H. Yang and T. C. Wen, *J. Appl. Electrochim.*, **24**, 166 (1994).
53. H. A Menezes and G. Maia, *J Electroanal Chem*, **586**, 39 (2006).
54. J. F. R. Nieto, R. I. Tucceri, and D. Posadas, *J. Electroanal. Chem.*, **403**, 241 (1996).
55. J. M. Ortega, *Thin Solid Films*, **371**, 28 (2000).
56. F. J. R. Nieto and R. I. Tucceri, *J. Electroanal. Chem.*, **416**, 1 (1996).
57. M. A. Goyette and M. Leclerc, *J. Electroanal. Chem.*, **382**, 17 (1995).
58. T. Ohsaka, S. Kunimura, and N. Oyama, *Electrochim. Acta*, **33**, 639 (1988).
59. S. S. M. Hassan, M. L. Iskander, and N. E. Nashed, *Talanta*, **32**, 301 (1985).
60. Z. Wang, X. Li, Y. Wu, Y. Tang, and S. Ma, *J. Electroanal. Chem.*, **464**, 181 (1999).
61. H. J. Salavagione, J. Arias, P. Garcés, and E. Morallń et al., *J. Electroanal. Chem.*, **565**, 375 (2004).
62. G. Socrates, *Infrared and Raman Characteristic Group Frequencies*, third ed., Wiley, New York, 2001.
63. Q. Yanga, Y. Zhanga, H. Li, Y. Zhanga, M. Liua, J. Luoa, L. Tana, H. Tanga, and S. Yaoa, *Talanta*, **81**, 664 (2010).
64. N. P. G. Roeges, *A Guide to the Complete Interpretation of Infrared Spectra of Organic Structures*, Wiley, Chichester, 1994.
65. J. Zhang, D. Shan, and S. Mu, *J. Poly. Sci., A. Poly. Chem.*, **45**, 5573 (2007).